Polynomial regression, Area and Length based filtering to remove misclassified pixels acquired in the crack segmentation process of 2D X-ray CT images of tested plaster specimens

Ujjal Kumar Bhowmik, Tyler Cork
Electrical Engineering and Computer Science Dept.
Catholic University of America, Washington DC, USA
Email: bhowmik@cua.edu

Nick W. Hudyma, School of Engineering,
University of North Florida.
Jacksonville, FL-32224, USA

***Abstract*—This work presents an effective and robust technique to remove misclassified pixels acquired in the crack segmentation process of 2D X-ray CT images of tested plaster specimens. Cracks have distinct properties, such as they are fairly piece-wise linear, and they have certain area and length ratios, which can be used to remove misclassified pixels from cracks segments. In this paper a combination of polynomial regression and area-based, length-based filtering scheme is applied to remove undesired pixels from the 2D CT images of plaster specimen. With the help of experimental results the effectiveness and robustness of the proposed technique are verified.**

Keywords—: computed tomography (CT), local entropy based thresholding, polynomial regression based filtering, area-based filtering, length-based filtering.

I. INTRODUCTION

Pores inside rocks, regardless of size, shape and location, have detrimental effects on the strength, stiffness and other physical properties of rocks [1]. In order to investigate the strength and stiffness of rocks, a test specimen is tested under compressive force in a universal testing machine. As the force increases, it reaches to the critical point when cracks develop inside the specimen. With continued loading the cracks coalesce and eventually the specimen fractures. Precise segmentation of cracks is essential for analyzing the strength, stiffness and other physical properties, such as permeability to gas or fluids, of rocks. Three dimensional (3D) computed tomography (CT) has recently been widely used in the field of geo-engineering to analyze and characterize the internal structures of rocks [2-4]. 3D CT images are formed from a stack of very thin cross-sectional slices of 2D CT images taken along the vertical direction of the test specimen [5]. In this research, 3D CT scanning is performed on a set of tested plaster specimen to visualize and analyze cracks.

Cracks in multi-phase materials, such as natural rocks, have lower reflectance compared to the other internal structure, which makes it difficult to correctly identify and segment cracks from CT images [6]. Crack detection and segmentation can be categorized as a problem of edge detection in image processing. However, the most of widely used edge detection based techniques, such as different thresholding techniques [7-8], gradient or higher derivative based methods (e.g. Canny, Sobel and Prewitt edge detection methods) [9], do not provide satisfactory results because of crack's poor local contrast. Several morphological based techniques have recently been introduced to segment cracks in x-ray CT images [3]. However, choosing proper structuring elements is a difficult problem in morphological analysis.

In medical imaging, the problem of segmenting blood vessel in retinal images is similar in nature to the segmentation of cracks in X-ray CT images of rock cross section. Blood vessels in retinal images, like cracks in rock, have lower reflectance compared to the background [10]. Chabwimaluang et. al. [11] developed a three-step algorithm to successfully segment blood vessels from retinal images. The process start with a 2D Gaussian matched filtering to enhance the prominence of blood vessels [10]. Second, a local entropy based scheme, which takes in to account the spatial distribution of gray-level and can preserve the spatial structures in binarized images, is applied to distinguish cracks from background. And finally a length filtering scheme is used to remove small segments of misclassified pixels. The above algorithm works well for enhancing the local contrast associate with cracks and thereby distinguishing cracks from the multi-phase crack background. However, the misclassified pixels acquired in this process are very dominant. A simple length filtering is not sufficient to remove unwanted pixels. Thus a combination of morphological-based operators, length and box filtering has been introduced to remove misclassified pixels from the 2D CT images of tested plaster specimen [12]. The above modified algorithm still poses difficulty in distinguishing between the micro-pores and the hairline cracks (i.e. the tipping point of cracks) for which the inherent tradeoff between the length filtering sensitivity and the images' signal-to-noise ratio limits the success. To circumvent this problem, some of the distinct physical properties of cracks, such as cracks are piece-wise and fairly linear features which can be modeled by polynomial regression and cracks have certain length to width ratio and depending upon the slope of the crack it will have certain area to envelope ratios, which can be modeled and incorporated in the algorithm. From empirical analysis, a combination of polynomial regression, area and length based filtering scheme is introduced in this paper. Experimental results validates the effectiveness and robustness of the proposed algorithm.

The remainder of the paper is organized as follows. Section II briefly describes the test specimen and the CT scanning mode used in this research. For the completeness of the paper, section III represents a short review of the 2D Gaussian matched

978-1-4673-9795-7/15 $31.00 © 2015 IEEE
DOI 10.1109/CSCI.2015.141

filtering and local entropy based filtering scheme. Section IV, elaborately discusses the proposed polynomials regression, area and length based filtering technique with the help of empirical analysis and experimental results. Section V discusses the challenges and future works and finally Section VI concludes the paper.

II. Test Specimen And The CT Scanning

The test specimens used in this research are made from plaster of paris. To mimic the presence of macro-pores in rocks, several regular shaped Styrofoam inclusions, such as spheres, cubes, egg, and truncated cones, are placed inside the plaster of paris [1]. Micro-pores are naturally created because of the presence of tiny air bubbles. Each specimen was tested under unconfined compression conditions until failure. Then the test specimens were then CT scanned in the UF-SHANDS Health Science Center in Jacksonville, Florida [1]. A 64-slice, dual X-ray tube medical CT scanner (Seimens Medical Solutions, Forchheim, Germany) is used for this research. As shown in figure 1, test specimens are placed on the scanner bed such that the cylinders' z-axis are aligned with that of the scanner. Cross-sectional images of the test specimens are reconstructed at a slice thickness of 1mm with in plane spatial resolution of 0.4 mm × 0.4 mm. Two such cross-sectional images are shown in figure 2. For each test specimen 336 cross-sectional images are saved. When these 2D CT images are stacked on top of one another and a suitable interpolation technique is applied, the 3D volumetric image is created (Figure 3). It is clearly evident that the cracks that are visible in the cross-section images are almost invisible in the 3D volumetric images. In this paper, the proposed algorithm is applied on each of the 336 cross-sectional images of a test specimen and the 3D structure of the cracks are made clearly visible in the volumetric image of the test specimen. In following sections the step by steps methods for segmenting cracks and removing misclassified pixel are explained with the help of experimental results.

Figure 1. CT scanning of plaster specimen

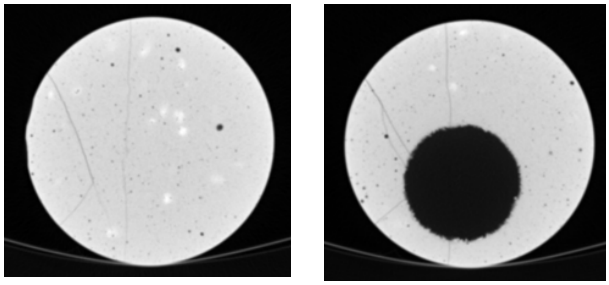

Figure 2. CT image of specimen cross-section

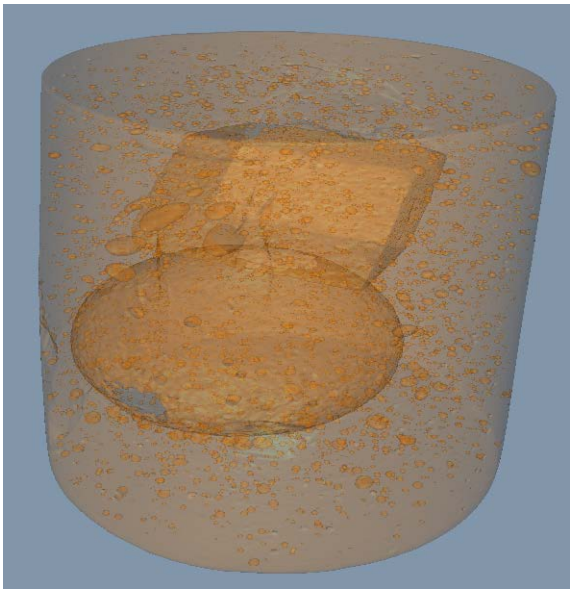

Figure 3. 3D CT image of the test specimen

III. 2D Matched-filtering and Local Entropy-based thresholding

It is clearly evident from figure 2 that cracks have lower reflectance compared to their neighbor and cracks almost never have ideal step edges. Cracks' small curvature and the anti-parallel lines can well be represented by a piece-wise linear segment. The gray-level intensity profiles of cracks resemble the inverse Gaussian shaped curve. Thus to enhance the local contrast of cracks, a two-dimensional Gaussian matched filter kernel, as shown in eqn. (1), is applied on the original images.

$$f(x,y) = -e^{-\frac{x^2}{2\sigma^2}}, \text{ for } |y| \leq L/2 \qquad (1)$$

where L is the segment for which the crack is assumed to have a fixed orientation. The direction of the crack is assumed to be aligned along y-axis. However, since cracks may be oriented at any angle, the kernel needs to be rotated for all possible angles [12]. Here, a set of 24 kernels of size 8×7 pixels are applied on the original image (I.e. the kernel is rotated by ±7.5º). The effectiveness of the 2D matched filtering is shown in Figure 4(b), where the original image and the filtered image are shown

side by side. It clearly evident the matched filtered CT image has improve the local contrast of crack significantly.

Next step is to binarize the matched-filtered images. The success of a segmentation process depends upon proper choice of a threshold value to distinguish the cracks from the background. Considering the spatial distribution of gray level in a multi-phase material, such as natural rocks, a local entropy based thresholding scheme [10] is applied on the matched-filtered images. In the following, the local-entropy based thresholding technique is addressed very briefly [11].

Let, $Q = |q_{ij}|_{m\times n}$ be an $m\times n$ dimensional co-occurrence matrix of an image $f(l,k)$, which gives an idea about the transition of gray-level intensities (*i, j*) between the adjacent pixels. Thus, Q possesses the spatial structural information of an image. Depending upon the ways gray-level *i* follows gray-level *j*, different types of co-occurrence matrix are possible. For this research, we used an asymmetric co-occurrence matrix which has horizontally right and vertically lower transitions. Thus, q_{ij} is expressed as follows:

$$q_{ij} = \sum_{l=1}^{m}\sum_{k=1}^{n} \delta \tag{2}$$

$$\text{where } \delta = 1 \quad \text{if} \begin{cases} f(l,k) = i \quad \text{and} \quad f(l,k+1) = j \\ \text{or} \\ f(l,k) = i \quad \text{and} \quad f(l+1,k) = j \end{cases}$$

$$\delta = 0 \qquad \text{otherwise}$$

The probability of co-occurrence p_{ij} of gray levels *i* and *j* can therefore be written as,

$$p_{ij} = \frac{q_{ij}}{\sum_i \sum_j q_{ij}} \tag{3}$$

If $t,\ 0 \le t \le L-1$, is a threshold. Then t can partition the co-occurrence matrix into four quadrants, namely A, B, C and D (Figure 7).

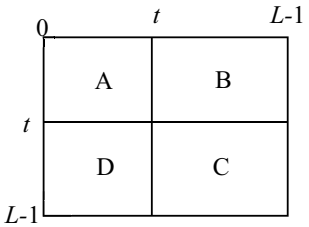

Figure 4. Quadrants of co-occurrence matrix

Let us define the probabilities of quadrants A and C as,

$$P_A = \sum_{i=0}^{t}\sum_{j=0}^{t} p_{ij}$$

$$P_C = \sum_{i=t+1}^{L-1}\sum_{j=t+1}^{L-1} p_{ij} \tag{4}$$

Normalizing the probabilities within each quadrants, such that the sum of probabilities of each quadrant equals one, we get the following probabilities of each cell quadrants:

$$P_{ij}^A = \frac{p_{ij}}{P_A} = \frac{q_{ij}}{\sum_{i=0}^{t}\sum_{j=0}^{t} q_{ij}}$$

Similarly,

$$P_{ij}^C = \frac{p_{ij}}{P_C} = \frac{q_{ij}}{\sum_{i=t+1}^{L-1}\sum_{j=t+1}^{L-1} q_{ij}} \tag{5}$$

The second-order entropy of the object can be expressed as:

$$H_A(t) = -\frac{1}{2}\sum_{i=0}^{t}\sum_{j=0}^{t} P_{ij}^A \, log_2 P_{ij}^A \tag{6}$$

Similarly, the second-order entropy of the background can be expressed as:

$$H_C(t) = -\frac{1}{2}\sum_{i=t+1}^{L-1}\sum_{j=t+1}^{L-1} P_{ij}^C \, log_2 P_{ij}^C \tag{7}$$

Thus, the total second-order local entropy of the object and the background can be expressed as:

$$H_T(t) = H_A(t) + H_C(t) \tag{8}$$

The gray-level corresponding to the maximum of $H_T(t)$ can be used as an optimum threshold for crack-background classification. The results of application of this local-entropy based thresholding is shown in Figure 5 (c). It is clearly evident that local-entropy based thresholding scheme has also extracted some microporous like structures as cracks. Thus to remove the misclassified pixels a morphological erosion operation followed by an eight-connected connected neighborhood based length filtering is applied. The results of the above process is shown in figure 5 (d & e). Although it appears that our previous algorithm has produced a very good results, careful investigation of the original images reveals the fact that the above technique has failed to detect and segment hair-line cracks on the left hand side of the square macro-pore. Decreasing the length filter's threshold can recover the hair-line cracks but it also acquired a significant amount of misclassified pixels, as shown in figure 5 (f). These misclassified pixels can be removed by choosing a larger threshold value for length filter, but choosing a larger threshold would again remove the hair-line crack segments. The following section discusses the steps proposed in this research to tackle this problem.

IV. A Combined Polynomial Regression , Area and Length Based Filtering Algorithm

Crack segments are fairly piece-wise linear which can be represented by 1st and 2nd order polynomials. Thus to distinguish between the crack segments and the unwanted pixels segments, a polynomial regression filter can be applied

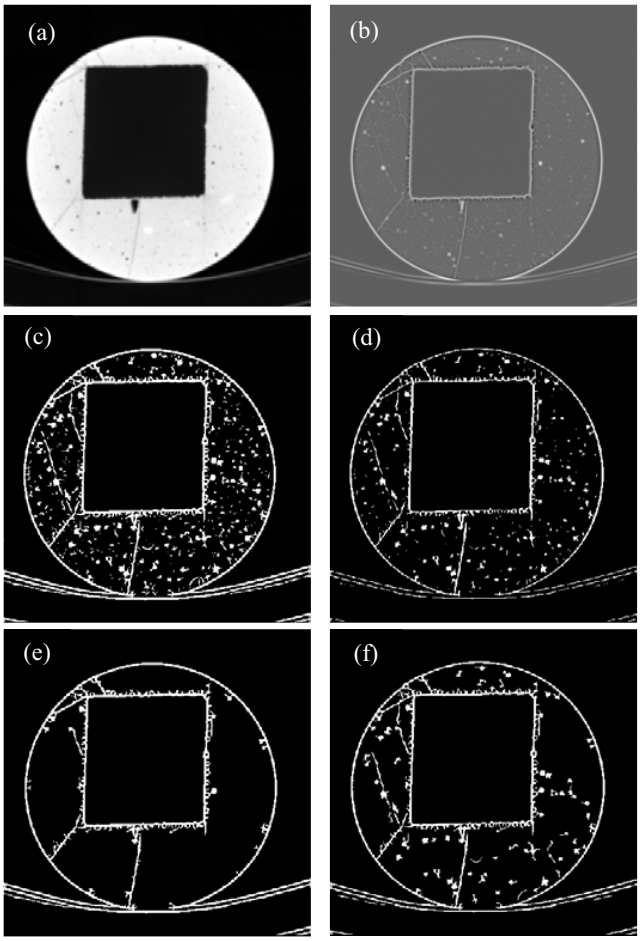

Figure 5. (a) Original cross-section, (b) Matched-filtered output, (c) Local-entropy based thresholding, (d) Erosion applied on thresholded image, (e) Output image after length filtering, (f) Output image for smaller threshold in length filter

on each connected segment. By choosing a proper value of coefficient of determination (i.e. r^2, as shown in eqn. 9) the unwanted pixel segments can easily be isolated from the crack segments.

$$r^2 = 1 - \frac{\sum(y_i - \hat{y}_i)^2}{\sum(y_i - \bar{y})^2} \quad (9)$$

where y_i is the data points of pixel segments, $\hat{y}_i$ is the prediction of the least square fit and $\bar{y}$ is the arithmetic mean of the data points. However, choosing the proper value of r^2 is a difficult task. From observation it is seen that for some values of r^2 within a range 0.6 to 0.8, some cracks show the same property of the other connected regions. Moreover, the size of the connected region also has a strong correlation with the value of r^2. Thus, the ratio of crack's envelop to its area (which is termed as area ratio) and ratio of crack's length to its width (which is termed as length ratio) are considered along with r^2 to filter out background noises (i.e. unwanted pixel segments) first. From empirical observation, different values of r^2, length ratio and area ratio are chosen for different sizes of the connected regions to remove background noises.

The process starts with the connected regions of sizes in between 15 and 45 pixels. It is observed that for this sizes of the connected regions, the (length ratio > 0.6) and (area ratio > 0.3), which resembles pretty much a rounded object, are for sure background noises. It is also observed that regardless of the values length and area ratios any connected region which has $r^2 < 0.2$ is for sure background noise. It is to be noted that crack segments which are perfectly aligned to either x-axis or y-axis (which is very unlikely) can have large area ratio. It is also to be noted that for the above range of the connected regions, smaller area ratio, length ratio and larger determination of coefficient (e.g. area ratio <0.3, length ratio < 0.6, and $r^2 > 0.8$) do not preclude that the connected regions do not have any noise. The best way to isolate these noises is to first identify the for sure crack segments and then extrapolate these detected crack segments to connect them with their respective broken segments. Thus, after removing the for sure background noises, the next task is to detect for sure crack segments by checking if the connected regions of the above range have either (very small area ratio && length ratio) or (very high r^2). From empirical observation, it is found that for (area ratio < 0.2 && length ratio < 0.3) or ($r^2 > 0.85$) are highly probable of being crack segments. Once these crack segments are detected, each of them is tested whether a 1st order polynomial or a 2nd order polynomial best represents the crack. The higher coefficient value for each crack segment is used to extrapolate the crack segment about three pixels at both ends of the crack segment. The output for this processing step is shown in figure 6 (a). From figures 6 (a), it is evident that the for sure noise segments are removed and the for sure crack segments are extended to their ends.

The same technique is sequentially applied to all other larger segments. As can be seen in figure 6 (b) (in which the connected regions of sizes in between 45 and 75 pixels are considered) and figure 6(c) (in which the connected regions of sizes in between 75 and 150 pixels are considered), the larger crack segments are connected to the smaller crack segments.

After the crack segments are detected and connected with their broken segments, the removal of the remaining background noises becomes easier. As now a suitable value of coefficient of determination can be chosen to remove noise from the image. From empirical observation, $r^2 < 0.7$ is chosen as the background noise. As shown in figure 6 (d) that most of the smaller segments of sizes in between 5 and 20 pixels are removed from the background. From figure 6 (d), it is also observed that because of the extrapolation in the previous stages, the crack like segments are connected together and become visible on the background along with other dust like noise particles. The dust like noise particle can easily be removed by using an empty widow of size 28×30 pixels. The window is scanned over the image and all the dust particles that are fully contained inside the window and the window boundary does not touch the other pixels, are removed from the image. Figure 6 (e) shows most of the dust like particles are removed from the image.

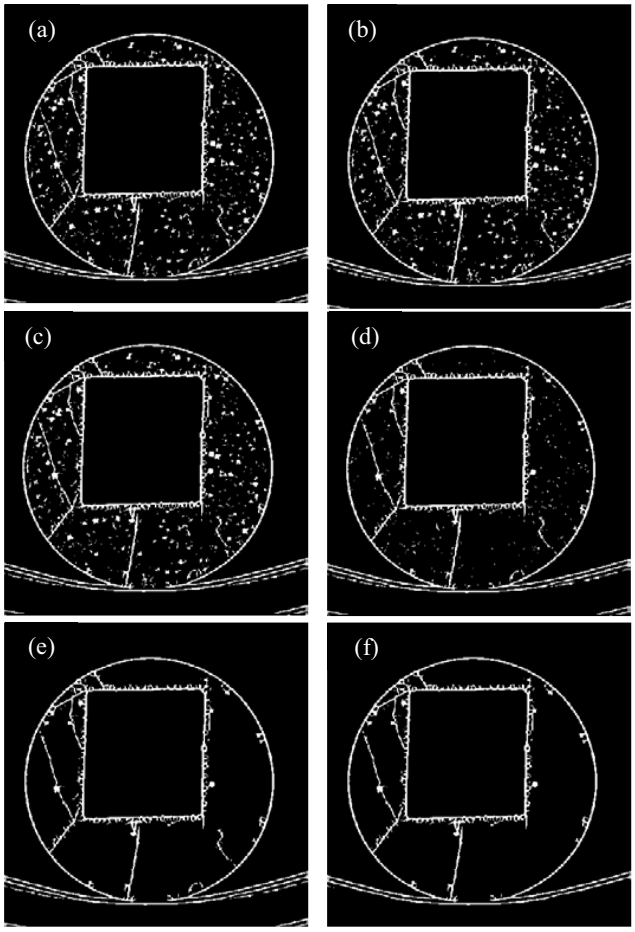

Figure 6. Binarized cross-sectional CT images showing the expected outcomes at different stages of a combined polynomial regression, area and length based filtering algorithm

Now to remove the remaining crack like connected segments, all the connected region of sizes in between 5 and 60 pixels are tested if their coefficient of determinations are less than 0.65. Any segment with $r^2 < 0.65$ (which is chosen from empirical analysis) is a good candidate for removal from the image as noise. For segments with $r^2 > 0.65$, the neighborhood of both ends are checked to see if they are close to any of the for sure crack segment detected in the previous stages. In case a neighboring crack is detected, the slope of the tested segment is compared with neighboring crack. If the slopes are within certain range (from empirical observation, it is observed that, slopes within 80% of one another), the tested segment is considered as good candidate for crack, otherwise it is removed from the image. From figure 6 (f), it is clearly evident that crack like noise segments are removed from the image. After removing these crack like segments, it left behind some residual dust particles, which is also be removed using the empty window as discussed before.

The above crack detection and noise removal technique is applied to all the 336 cross-section CT images of the test specimens. All the processed images are stacked on top of one another and an application software, Voxler 3, is used to create the 3D image of the test specimen. As shown in figure 7, the cracks along with the inclusions are easily visible in the volumetric images taken at different angle of the test specimen. Now to get a clear view of the cracks, the outer boundary is removed from the 2D images (figure 8) and the resultant 3D images are shown in figure 9.

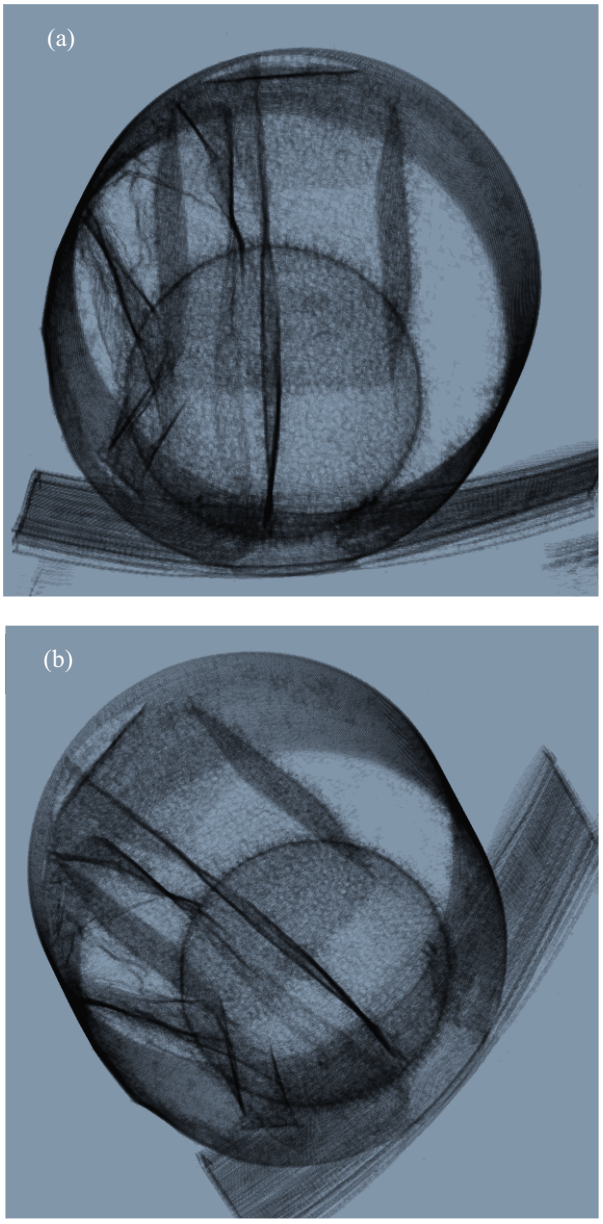

Figure 7. Three-dimensional images of the test specimen showing the cracks along with inclusion in the test specimen.

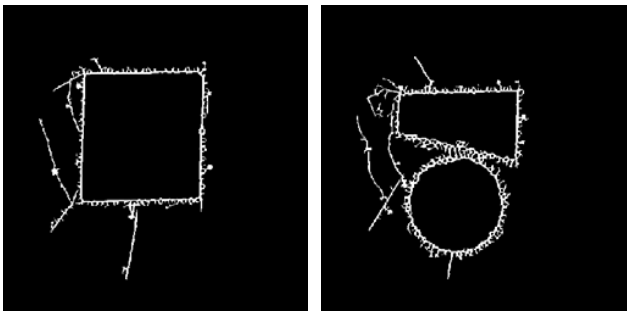

Figure 8. Boundary-less cross-sectional x-ray CT images of the test specimens used for boundary less 3D images

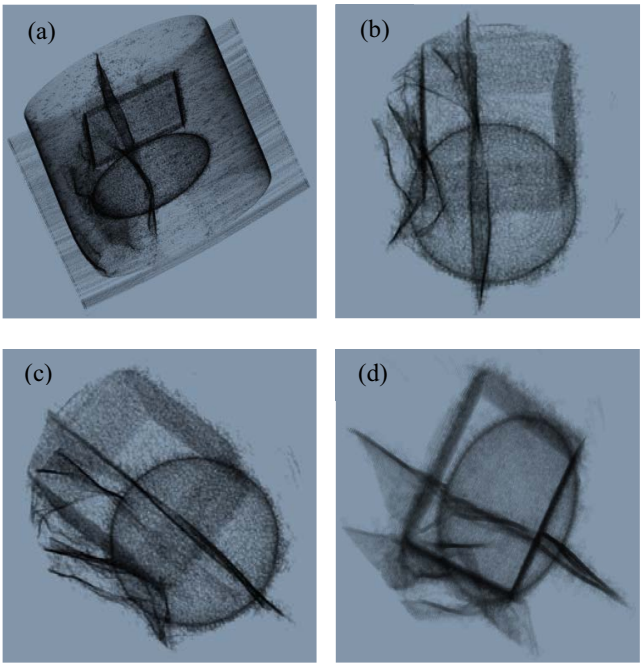

Figure 9. (a) 3D image of the test specimen showing the crack and inclusions. (b)-(c) Boundary-less 3D images and (d) smooth boundary-less 3D image of the test specimen.

V. Challenges and Future Works

From boundary-less 3D images (as shown in figure 9 (b & c), it is clearly evident that the cracks planes are accompanied by some protrusion which would make it difficult to quantitatively analyze cracks properties (e.g. measuring crack volume, which is a very important parameter used in charactering the physical properties of rocks). After carefully investigating all the 336 segmented 2D cross-sectional images, it is discovered that each crack segments is accompanied by some sort of protrusions on it. To minimize the protrusion effect, a smoothing filter (for our case a simple average filter) is applied on the 2D images and a 3D image is created from the smooth 2D images, as shown in figure 9(d). Although the smoothed 3D image gives better visualization of the cracks, it is not free from protrusion effect. Removing protrusion from 2D images would certainly enhance the quality of the 3D images of cracks. In our future endeavor efforts will be made to solve this problem.

VI. Conclusion

In this paper an effective and robust technique is designed and implemented to remove undesired pixel segments acquired during the crack segmentation process of 2D X-ray CT images. The proposed technique incorporated some distinct physical properties of cracks in the algorithm to isolate unwanted pixel segments from cracks. The algorithm consists of a combination of a polynomial regression based filter (which represents crack segment as piece-wise fairly linear segment), area-based filter (which represents crack's probable area ratio) and length-based filter (which represents crack's probable length ratio). Experimental results demonstrate the validity of proposed technique. Although the algorithm works very well in removing unwanted isolated pixel segments from the 2D X-ray CT images, it produces some protrusion effects on the cracks. In our future works, emphasis will be given to remove the protrusion effects and develop a mathematical model to analyze the physical properties of 3D crack segments.

References

[1] N. Hudyma, K. Johnson, C. Sherman, and M. Maclaughlin, "Comparisons of 2D Imaging Techniques for Internal Macropores Characterization,"ARMA.10-376

[2] J. Behnsen, O. O. Blake, R. J. Cernik, P. J. Withers, Proc. Of Identifying microcracks in multi-phase crystalline rocks by X-ray CT, University of Applied Sciences, Wels, Austria, 2014.

[3] E. R. Urbach, M. Pervukhina, and L. Bischof, "Segmentation of Cracks in Shale Rock," Mathematical Morphology and Its Applications to Image and Signal Processing Lecture Notes in Computer Science, pp. 451-60, 2011.

[4] B. Robbin, J. Nichols, R.L. Mokwa, B. Khun, M.M. Maclaughlin, and N. Hudyma, "Quantifying Internal Macroporosity using CT Scanning," ARMA 11-264

[5] A.C. Kak, M. Slaney, Principle of Tomographic Imaging, IEEE Press, 1999

[6] F.D.E. Latief, U. Fauzi, and S. Feranie, "Digital Isolation Technique for Reconstruction and Visualization of Cracks in Micro-CT Images of Geothermal Reservoir Rock," Microscopy and Analysis, pp. 13-7, 2012.

[7] I. E. Abdou and W. K. Pratt, "Quantitative design and evaluation of Enhancement/thresholding edge detectors," Proc. IEEE, vol. 67, pp. 753-763, May 1979.

[8] R. M. Haralick, J. S. J. Lee, and L. G. Shapiro, "Morphological edge detection," IEEE J. Robotics Automat., vol. RA-3, pp. 142- 155, Apr. 1987.

[9] D. Marr and E. Hildreth, "Theory of edge detection." Proc. Rry. Soc. London, Ser. B, vol. 207, pp. 187-217, 1980.

[10] S. Chaudhuri, S. Chatterjee, N. Katz, M. Nelson, and M. Goldbaum, "Detection of blood vessels in retinal images using two-dimensional matched filters," IEEE Trans. Med. Imag., vol. 8, no. 3, pp. 263–269, 1989.

[11] T. Chanwimaluang, G. Fan , and S.R. Fransen, "Hybrid retinal image registration," IEEE Trans. Inf. Tech. Bio., vol. 10, no. 1, pp. 129-–142, 2006.

[12] U. K. Bhowmik, D. Mandala, N. W. Hudyma, O. P. Kreidl, and A. Harris, "Segmentation of Cracks in X-ray CT Images of Tested Macroporous Plaster Specimens," IEEE Southeastcon 2014, 2014.